ACI STRUCTURAL JOURNAL TECHNICAL PAPER

Title No. 121-S18

Prediction of Tensile Properties of Ultra-High-Performance Concrete Using Artificial Neural Network

by Amjad Y. Diab and Anca C. Ferche

A multilayer perceptron artificial neural network (MLP-ANN) was developed to calculate the cracking stress, tensile strength, and strain at tensile strength of ultra-high-performance concrete (UHPC), using the mixture design parameters and strain rate during testing as inputs. This tool is envisioned to provide reference values for direct tension test results performed on UHPC specimens, or to be employed as a framework to determine the tension response characteristics of UHPC in the absence of experimental testing, with minimal computational effort to determine the tensile characteristics. A database of 470 data points was compiled from 19 different experimental programs with the direct tensile strength, cracking stress, and strain at tensile strength corresponding to different UHPC mixtures. The model was trained, and its accuracy was tested using this database. A reasonably good performance was achieved with the coefficients of determination, R^2*, of 0.91, 0.81, and 0.92 for the tensile strength, cracking stress, and strain at tensile strength, respectively. The results showed an increase in the cracking tensile stress and tensile strength for higher strain rates, whereas the strain at tensile strength was unaffected by the strain rate.*

Keywords: artificial neural network (ANN); cracking stress; machine learning; multilayer perceptron (MLP); tensile strength; ultra-high-performance concrete (UHPC).

INTRODUCTION

Ultra-high-performance concrete (UHPC) is widely recognized as a cementitious composite with a discontinuous pore structure, incorporating steel fiber reinforcement.[1] UHPC is attracting increased use due to its outstanding material properties, such as high compressive strength, high tensile strength, excellent crack control properties, self-consolidating workability, and exceptional durability in aggressive environments.[2,3] These characteristics make it possible, in some cases, to significantly reduce or eliminate conventional reinforcement and allow the use of thinner concrete sections in practical applications.[4] As a result, UHPC becomes an advantageous choice in high-performance applications, such as long-span precast pretensioned elements, bridge decks, offshore platforms, nuclear power plant buildings, and blast- and impact-resistant structures.[5]

UHPC was introduced for the first time in 1994,[6,7] and it differs from ordinary concrete in various aspects, including low water-cement ratio (w/c), the incorporation of silica fume with optimized quantities of portland cement, fine aggregates, and the absence of coarse aggregates.[8] Recent efforts have concentrated on the formulation of UHPC mixtures that are more economical and have enhanced sustainability characteristics,[9-17] resulting in the incorporation of additional supplementary cementitious materials (SCMs) within the UHPC mixture, such as fly ash (FA), granulated blast-furnace slag (GBFS), metakaolin, and the use of limestone powder.[13-16]

The incorporation of fiber reinforcement in the UHPC mixture, such as steel or propylene fibers, results in post-cracking ductility and enhanced energy absorption capacities that are not superior to conventional concrete. As a result, UHPC provides a reliable solution for cases when high strain rates are generated by impact loads, blast, and seismic loading.[18] While the strain-rate sensitivity of conventional concrete is known to be strongly dependent on the quality of the concrete mixture,[19,20] for fiber-reinforced concrete, the strain-rate sensitivity is highly influenced by additional factors, such as fiber volume percentage, fiber type, and fiber bond strength.[21,22] Several studies examined the tensile behavior of various UHPC mixtures at varying strain rates[21-26] and shed light on its influence on mechanical properties such as the cracking stress, tensile strength, and the strain at tensile strength. The findings demonstrate that UHPC has a complex behavior, depending on the strain rate, and the mixture composition in terms of SCMs, fiber reinforcement type, and the overall mixture design.

Numerous empirical models were developed to estimate the dynamic increase factor for UHPC,[27,28] all indicating that the response of UHPC is even more sensitive to the strain rate than conventional concrete due to the presence of the fiber reinforcement.[29] In addition, the low w/c and inclusion of SCMs promote the formation of a denser structure,[30,31] which in turn increases strain-rate sensitivity according to the Stefan effect.[32]

The direct tension tests, splitting tensile tests, and flexural tests are the three most commonly used testing procedures for characterizing the behavior of UHPC in tension.[32-34] The experimentally measured tensile strength values vary depending on the tensile stress distribution and boundary conditions corresponding to these different tests.[35] Among them, the direct tension test presents the advantage of a uniform stress condition and the ability to record the complete stress-strain response before and after cracking. As such, in terms of insight for material characterization, the authors view the direct tension test as superior compared to

ACI Structural Journal, V. 121, No. 2, March 2024.
MS No. S-2022-248.R1, doi: 10.14359/51740245, received June 29, 2023, and reviewed under Institute publication policies.

the splitting tensile and flexural tests. Nevertheless, it presents well-known challenges pertaining to the execution of the test, especially, ensuring a uniform uniaxial stress condition before and after cracking.

Typically, UHPC mixtures are classified according to their post-cracking stress-strain response into strain-softening or strain-hardening materials.[36] Figure 1 displays typical strain-softening and strain-hardening behavior. The cracking stress (f_{cr}) is defined as the stress at which the first crack occurs, the tensile strength (f_t') is defined as the maximum tensile stress, and the strain at tensile strength (ε_t'), refers to the strain corresponding to f_t'. The work presented herein was performed to provide values for the cracking stress, tensile strength, and the strain at peak stress of UHPC mixtures tested under different strain rates, based on information related to the mixture design.

Overall, the tensile response of UHPC is highly influenced by numerous factors, including the *w*/*c*, SCMs-to-cement ratio, high-range water-reducing admixture-to-cement ratio, and fiber volume and type, in addition to the tensile strain rate. These factors were observed from previous experimental programs to have a higher impact on the tensile strength than the compressive strength of UHPC; consequently, the empirical approaches commonly used to estimate the tensile strength of conventional concrete as a function of the compressive strength only would not be adequate for UHPC.[37] For example, the fiber volume of a mixture was shown to have a higher degree of influence on the tensile strength than the compressive strength.[25-27] At the same time, in the design of structural elements cast with UHPC, the tensile strength of the UHPC material is usually considered as a contributing factor to the strength of the element. Therefore, there is an urgent need for a reliable approach to determine the tensile strength of UHPC. The work presented herein is an effort toward this endeavor. Previously, multilayer perceptron artificial neural network (MLP-ANN) models have been effectively used in a variety of UHPC applications, including the prediction of the mechanical properties of UHPC mixtures, such as their compressive strength, modulus of elasticity, flowability, and porosity.[38-42] The goal of this research was to develop an MLP-ANN framework for calculating the cracking stress, tensile strength, and the strain at tensile strength of UHPC, using as inputs the parameters found to be influential, as previously mentioned. This tool is envisioned to provide reference values for direct tension test results performed on UHPC, or to be employed as a framework to determine the tension response characteristics of UHPC in the absence of experimental testing.

RESEARCH SIGNIFICANCE

In contrast to structural elements cast with conventional concrete, the tensile strength of UHPC is typically a design factor contributing to the strength of UHPC members. Determining the tensile strength of UHPC, however, poses several challenges and introduces a degree of uncertainty that is not yet well understood. An MLP-ANN model was developed for calculating the cracking stress, tensile strength, and the strain at the tensile strength of UHPC using as input information pertaining to the mixture design. To the authors' best knowledge, no previous studies address the prediction of the aforementioned tensile properties of UHPC using MLP-ANN. The authors believe that the procedures proposed in this study will be of general interest to the practicing engineers and standards committees, with the goal of accelerating the widespread adoption of UHPC components in structural applications. The MLP-ANN presented herein was developed based on a database of 470 data points, and it is hoped to be used to provide a baseline for the experimentally determined tensile properties in an effort to reduce the inherent uncertainty associated with tensile testing, or to be employed as a framework to establish the tension response characteristics of UHPC in the absence of experimental testing.

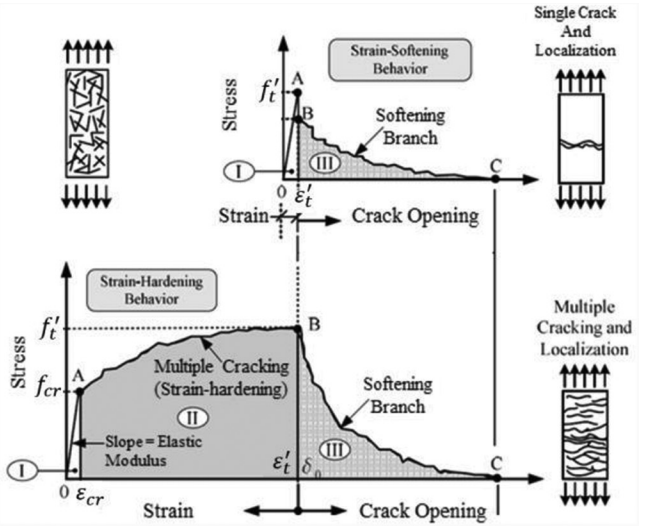

Fig. 1—Typical UHPC stress-strain response in tension: (a) strain-softening behavior; and (b) strain-hardening behavior.[36]

ARTIFICIAL NEURAL NETWORKS

Overview

An artificial neural network (ANN) is a data processing paradigm inspired by the biological neural system. This paradigm is reliant on the shape of the information processing system. ANNs have a mechanism for extracting interconnections from complex data and can be used to discover patterns and identify trends that would typically be obscured.[43] An ANN is a type of nonlinear function approximator that creates mapping between the input and output parameters. The network uses learning capabilities derived from the given inputs,[44] making this approach ideal for predicting the UHPC tensile properties due to the relatively large number of input parameters controlling these properties and the nonlinear relationship between the given inputs and outputs. A flowchart representing the general design and development procedure for an ANN is shown in Fig. 2.

The perceptron is the most basic type of neural network architecture and is being used in numerous advanced neural network applications. It is composed of multiple weighted connections and an activation function that connects the input and output layers.[45,46] The activation function decides whether to activate the neuron based on the input values and their weights, as explained in the following section. The

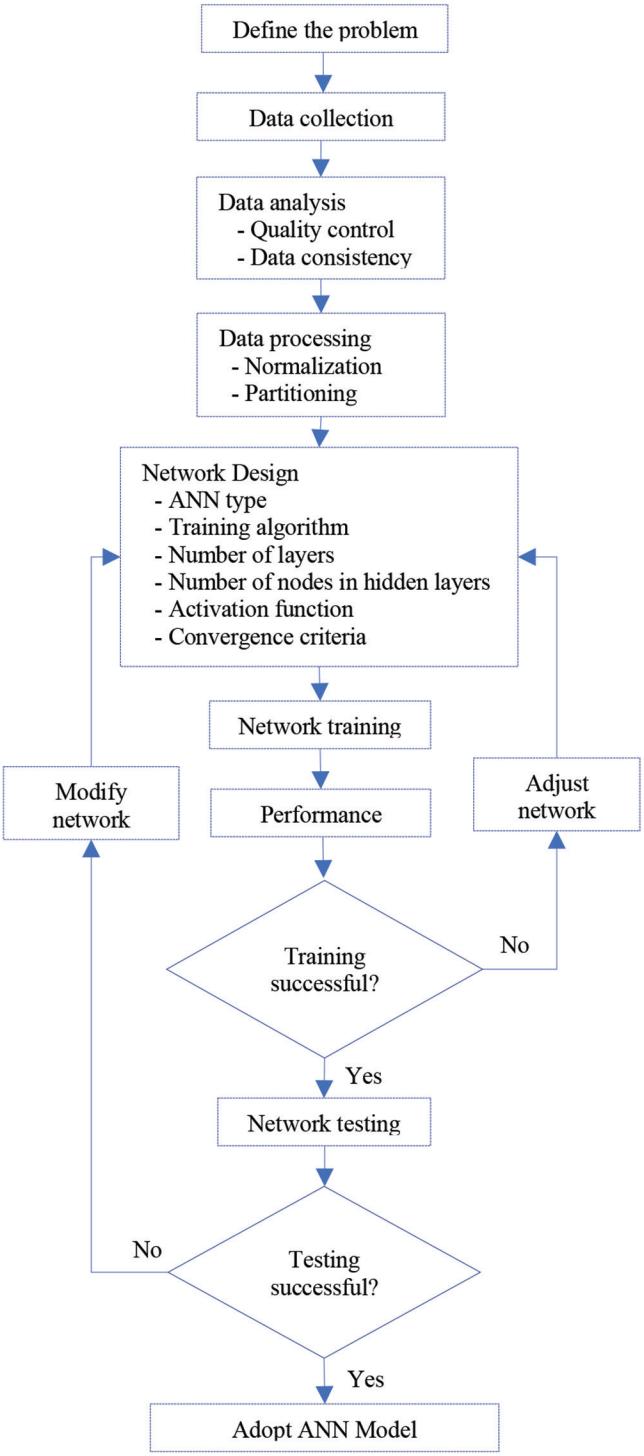

Fig. 2—ANN design and development procedure flowchart.

basic mechanism of the artificial neuron used in ANNs is shown in Fig. 3.

Feed-forward networks and recurrent networks are the two main types of ANNs. The MLP-ANN is one of the most widely used feed-forward ANNs,[47] and it represents a modification of Rosenblatt's perceptron model that includes hidden layers between the input and output layers. The goal of the architecture is to optimize the number of layers and neurons in each layer so that the network can solve the regression or classification problem with the given parameters.[48] Figure 4 shows the input layer variables, hidden layers, and output layer variables in a schematic diagram of the preliminary layout of the MLP-ANN structure used in this study. The algorithm was developed using the Python programming language.

Activation functions

The challenge with employing neural network architectures consists of the difficulty in designing algorithms that successfully learn patterns in data sets. Numerous strategies were explored to increase the effectiveness of these learning algorithms, such as normalizing the data points and optimizing the activation functions used in the ANN. An activation function determines whether to activate the given neuron, providing an output depending on the input values multiplied by their corresponding weights.

The hyperbolic tangent, sigmoid functions, and the rectified linear unit function (ReLU) are some of the most commonly used activation functions. The ReLU has been shown to be the most effective activation function for both regression and classification purposes.[49] The graphical representation of the ReLU activation function is depicted in Fig. 5; the function receives modified inputs, multiplying by their respective weights and adding the bias values. Finally, the neuron outputs a value depending on the weighted values of the inputs. The benefit of using the ReLU consists of its capacity to discard neurons with negative weights and biases in the learning process, allowing for a faster and more precise learning process. The ReLU function was employed as the activation function for the hidden layers in this study, whereas a linear activation function was used for the output layer.

Training model

The ANN's training phase is critical, and it represents a function minimization problem in which an error function is minimized, assisting in the selection of the optimal weights. Rumelhart et al.[50] developed one of the most widely used training algorithms, the backpropagation method for neural networks, in which the neural network procedure repeatedly customizes the weights of the connections in the network to minimize the difference between the actual output vector (experimentally measured tensile properties) and the predicted output vector (predicted tensile properties).

The backpropagation technique analyzes the information in two steps: initially, in the forward pass, it calculates the outputs and the error at the output layer. This is followed by the backward pass, as it updates the weights of the same units using the error at the output layer. This technique is repeated until the error converges to a minimum value, at which point the cost function is specified. For convergence, several optimization techniques are generally applied, including the schematic gradient descent[51-53] and the Adam optimizer.[54] In this work, the Adam optimizer was used as the optimization algorithm.

Model performance evaluation

After the training phase, the accuracy of the model was verified with respect to calculating the cracking stress, the tensile strength, and the strain at the tensile strength. The

root-mean-square error (RMSE) and coefficient of determination (R^2) were used as statistical parameters to determine the accuracy of the predictions of the model, calculated as shown in Eq. (1) and (2)

$$\text{RMSE} = \sqrt{\frac{\sum_{i=1}^{n}(Y_{pred} - Y_{ref})^2}{n}} \quad (1)$$

$$R^2 = 1 - \frac{\sum_{i=1}^{n}(Y_{pred} - Y_{ref})^2}{\sum_{i=1}^{n}(Y_{ref})^2} \quad (2)$$

where n is the total number of data points; Y_{pred} is the calculated value; and Y_{ref} is the experimental value.

The RMSE is one of the most frequently used error-index statistics.[55] RMSE compares experimental and predicted values and evaluates the square root of the mean residual error, indicating the error in units of the constituent of interest. The optimum RMSE value is zero, indicating a perfect match. The coefficient of determination (R^2) compares the accuracy of the model to that of a basic benchmark model, where the prediction is the mean of all samples.[56] The R^2 statistics are based on linear relationships between experimental and predicted values and may produce biased findings when the relationship is not linear or when the database contains numerous outliers. The value of R^2 is unity when there is equality between the observed and predicted values. A combination of the performance indicators described previously can provide an impartial estimate of the neural network models' prediction ability.

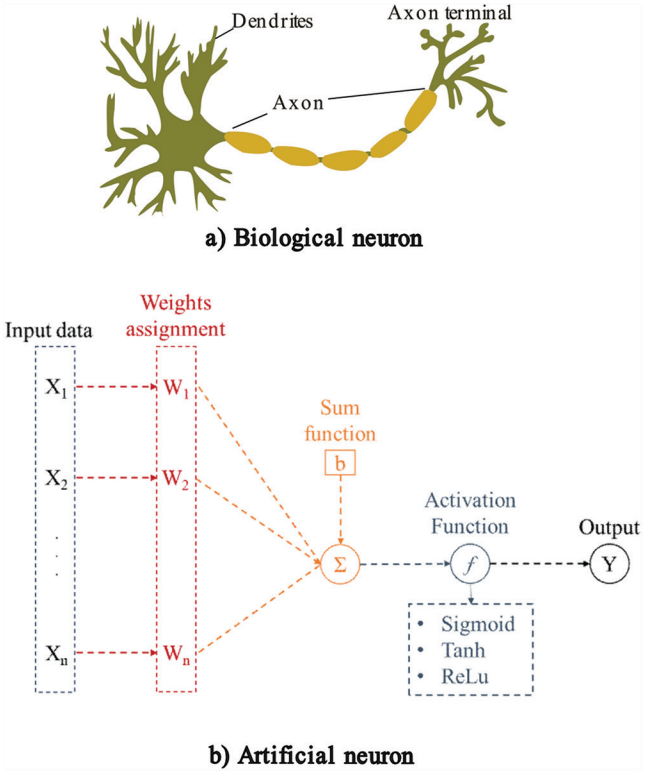

Fig. 3—Mechanism of artificial neuron depicting biological neuron.

DATABASE

Whereas recently, the focus in the literature has been primarily on the prediction algorithms in machine learning applications and the optimization of these algorithms, the importance of a dependable, representative, and sufficient database is oftentimes neglected, even though the database characteristics have a crucial role in developing a successful model. Sufficient data size is regarded as data that cover

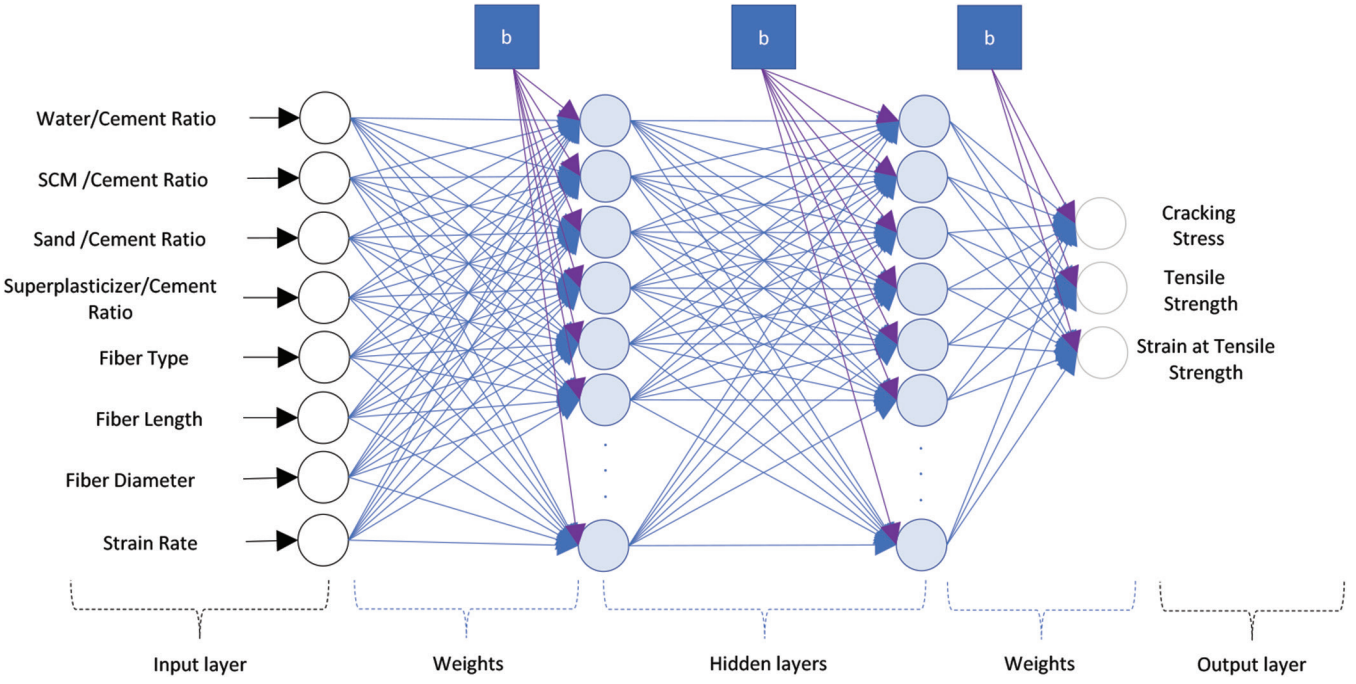

Fig. 4—Schematic representation of MLP-ANN.

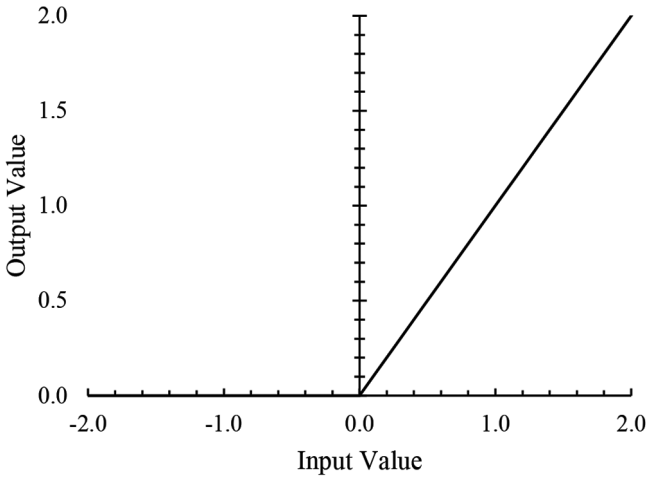

Fig. 5—Graphical representation of ReLU activation function.

all possible parameter combinations that determine the outputs the model is to predict, allowing the entire problem to be effectively simulated. A reliable database is especially important in the case of experimental databases, which frequently exhibit a considerable variance between results due to both unforeseen errors that were not accounted for while planning the experiment and inherent biases while implementing the experiment.

A database of 470 data points was compiled from 19 different experimental programs with the direct tensile strength,[18,25,26,57-72] cracking stress, and strain at the tensile strength of UHPC mixtures. These values were obtained from tests conducted on UHPC specimens that were tested under uniaxial tension at different strain rates. Table A1 in the Appendix summarizes the specimens compiled from the literature. Using this database, each input training vector was assigned 16 parameters, summarized in Table 1. The output vector includes the value of the tensile strength, cracking stress, and the strain at the tensile strength. The range, mean, and standard deviation values of the parameters included in the database are listed in Table 1.

A nonlinear relationship was found between the fiber aspect ratio (fiber length/fiber diameter) and the UHPC mechanical properties characterizing the tensile response. This is primarily due to the fact that the fiber diameter has a more pronounced influence compared to the fiber length.[29,66,72] For example, Park et al.[70] tested UHPC specimens cast with fibers having the same aspect ratio but different lengths and diameters and observed different tensile responses. As such, in this study, the fiber aspect ratio was disaggregated to capture the fact that the length and diameter of the fibers influence the tensile response differently and, therefore, need to be assigned different weights in the MLP-ANN model.

For the mixtures that contained fibers of the same type but with different lengths or diameters, a weighted average length or diameter was set as representative for the sample. The number of threads of the twisted fibers, the number of bends on hooked fibers, and the ultimate tensile strength of the fibers were not considered as parameters in the prediction model, as observations from experimental testing in the literature indicate they have negligible effects on the tensile strength properties.[66,72] Following similar reasoning, the influence of the curing regime and duration were also neglected in the formulation of the model, as were the constituents of the fine aggregate component, such as silica flour and glass sand.

The reliability of this database stems from the fact that its data points are based on experimental results reported in the literature rather than simulated values, which can often be subjective based on the models selected. A frequency assessment conducted on the database showed that the input parameters captured a reasonably acceptable range for the model to be accurate in predicting the dependent variables. This is illustrated in Fig. 6, which shows a pairplot distribution graph, constructed using Python's seaborn module.[73,74] Figure 6 allows the visualization of the given data such that the interrelationships between the different input and output parameters are illustrated. In addition, the range of the collected data is also displayed. For example, for the collected database, the average tensile strength of the UHPC mixtures is approximately 10 MPa and the *w*/*c* is approximately 0.2. These ranges can also help identify the limitations of the current database—for instance, more data are needed to fully analyze the effect of FA on the tensile properties of UHPC. This is illustrated by the frequency distribution plot for FA, with the majority of the data points having no FA in the mixture design. Only a minor portion of the data points have FA, with a percentage of up to 25% replacement. Overall, Fig. 6 illustrates that the constructed database covers a wide range of parameters that are used in UHPC mixtures. The relationships between the input and output parameters can also be visualized from Fig. 6. For example, for the tensile strength, analyzing the plot including the *w*/*c* and tensile strength, an inverse correlation can be observed. On the other hand, a positive correlation is revealed between the strain rate and tensile strength.

It should be noted that some of the concrete variables can be dependent on each other. Hence, the correlation coefficients between all possible variables have been derived and are presented in Fig. 7. Positive unity indicates a perfect positive correlation, negative unity shows a perfect negative correlation, and zero shows no correlation between the parameters. As expected, there is a strong positive correlation, with values higher than 0.75 between the strain rate and the cracking stress and tensile strength, whereas there is no clear correlation between the strain rate and the strain at tensile strength. In addition, the preliminary analysis indicates that the polyethylene fibers have a more pronounced influence on the strain at tensile strength of UHPC, compared to the steel fibers.

As part of data processing, outliers were identified and removed from the database. For the experimental studies that performed tests on multiple specimens of the same mixture design, the standard deviation and the mean values were calculated for the tensile properties. The experimental data with values that were higher or lower than twice the standard deviation difference from the mean value were considered outliers and were removed accordingly.

Table 1—Descriptive statistics of input and output variables in database

Parameter	Symbol	Units	Category	Min.	Mean	Max.	Standard deviation
Water-cement ratio	*w/c*	—	Input	190	22.2	35	4.25
Fly ash-cement ratio	FA/C	—	Input	0.0	1.5	25	5.4
Sand-cement ratio	Sa/C	—	Input	12.5	134	164	22.2
Silica fume-cement ratio	SF/C	—	Input	0.0	23.6	39	8.0
GGBFS-cement ratio	BFS/C	—	Input	0.0	5.0	107	19.5
High-range water-reducing admixture	S/B	—	Input	0.5	3.6	6.7	2.6
Straight fiber, %*	SF	—	Input	0.0	1.0	3	0.9
Straight fibers length	SFL	mm	Input	0.0	11.3	30	9.2
Straight fibers diameter	SFD	mm	Input	0.0	0.1	0.40	0.1
Hooked fiber, %*	HF	—	Input	0.0	0.26	3.6	0.6
Hooked fibers length	HFL	mm	Input	0.0	7.1	62.0	14.3
Hooked fibers diameter	HFD	mm	Input	0.0	0.1	0.9	0.2
Twisted fiber, %*	TF	—	Input	0.0	0.4	3.0	0.8
Twisted fibers length	TFL	mm	Input	0.0	4.9	30.0	9.6
Twisted fibers diameter	TFD	mm	Input	0.0	0.06	0.3	0.1
Polyethylene fibers, %*	PE	—	Input	0.0	0.2	2.1	0.6
Tensile strain rate	SR	s^{-1}	Input	0.00006	18.5	161	39.4
Tensile strength	TS	MPa	Output	3.8	17.3	68.1	9.6
Cracking stress	CTS	MPa	Output	4.8	11.3	32.7	4.8
Strain at tensile strength	STS	$\times 10^{-3}$	Output	0.2	11.8	80	13.2

*Fibers are provided by percentage of fiber volume to entire mixture volume.

Note: C is percentage relative to cement weight; B is percentage relative to total binder weight; 1 mm = 0.039 in.; 1 MPa = 145 psi.

Data normalization

Following the removal of outliers from the database, the next stage was data normalization. In general, the input and output data have different identities with no or minimal similarities. Data normalization removes the risk of neural network bias toward various identities. To prevent difficulties connected with the learning rate of the MLP-ANN, the min-max normalization method was used in this work[73]; data scaling between 0 and 1 was performed.

Data leakage

Data leakage is one of the main challenges facing machine learning applications[75]; it occurs when the data used to train a machine learning algorithm contains the information about the validation model that might not be available in the practical applications of the model. Data leakage can cause the machine learning algorithm to show good prediction results in both the test and training data sets but perform poorly in practical prediction applications.

There are mainly two types of data leakage[76]: feature and train-test leakage. Feature leakage is common in classification problems and occurs when one of the parameters used includes data that will not be available in the practical applications. Train-test leakage is more common in regression problems and occurs when training data has leaked information of the test data; this can be avoided by removing the randomization in sectioning the test and train ing sets to ensure that the algorithm is not trained on data similar to the one the algorithm is to be tested on. Train-test leakage was avoided by using different experimental programs in the training and testing phases.

Data fitting

Figure 8 depicts the three possible outcomes for data fitting. Underfitting occurs when the learning algorithm is unable to find a solution that fits the training examples well, while overfitting occurs when the learning algorithm finds an excellent solution for the training data but predicts unusual results in terms of new data other than the data for which it was trained. Overfitting can be a major issue in the machine learning process as it hinders the ability to generalize models. This can be caused due to a variety of reasons, such as presence of noise in the data set, insufficient data used for the training phase, or overly complex prediction algorithms.[77,78]

To avoid overfitting in the developed MLP-ANN model, the data was partitioned into two sets: training and test data sets. The training data set included 80% of the total data points and was used to aid the model in learning the prediction patterns, while the test data set comprised 20% of the total data. Underfitting would show the model having low accuracies in both the training and test data sets, while overfitting would show the model having high accuracy in the training phase with low accuracy in the test phase. Neither issue is observed for the model developed in this study.

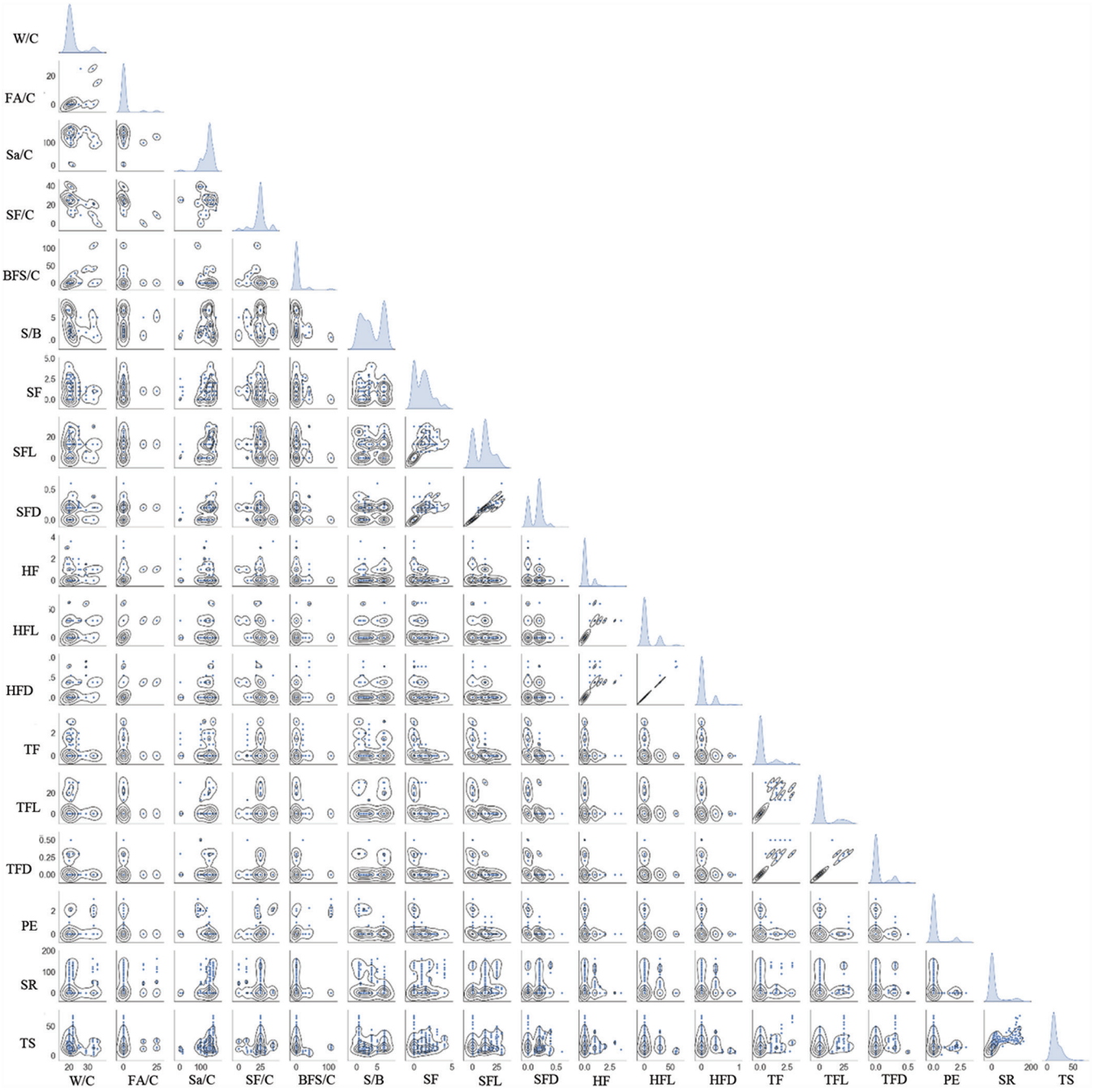

Fig. 6—Pairplot distribution analysis between database variables. (Note: Abbreviations are provided in Table 1.)

DISCUSSION OF RESULTS

The architecture of the MLP-ANN was developed to achieve the lowest mean squared error (MSE) in the development phase and the corresponding R^2 and RMSE when comparing the experimental and predicted results. Table 2 shows the corresponding MSE with the different number of neurons for the MLP-ANN model predicting the cracking stress, tensile strength, and the strain at tensile strength. Using a trial-and-error approach, testing neuron configurations with numbers ranging from five to 40 neurons, the optimum number of neurons converged to 25 neurons in each hidden layer, reaching the minimum MSE of 6.8, as shown in Table 2.

The results of the performance evaluation of the selected models are presented in Table 3; similar values were obtained in terms of the performance measures for the training and test sets discussed previously, indicating a proper performance of the MLP-ANN model developed. Figure 9 shows the comparison between the experimental and predicted results for the cracking stress, tensile strength, and the strain at tensile strength. The model shows accurate results in predicting the tensile strength characteristics based on the mentioned input parameters. In addition, the similarity of the R^2 and RMSE values between the training and test data sets indicates overfitting was not an issue in the prediction process, with no need for compensating techniques such as regularization.

Shown in Fig. 9 is the comparison between experimental and predicted values of the tensile properties, differentiating based on the strain rate employed during testing

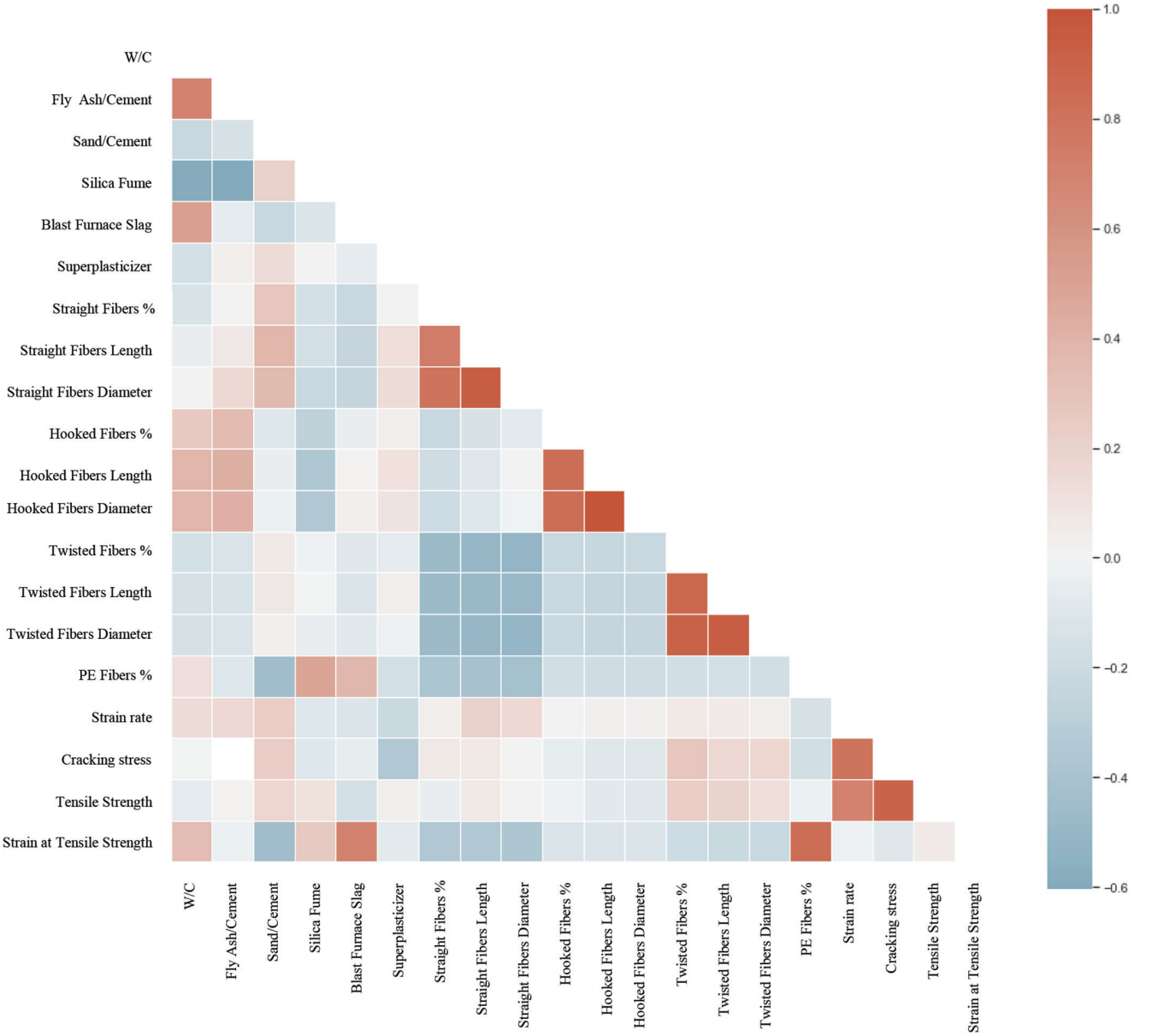

Fig. 7—Correlation analysis between database variables.

Table 2—Corresponding MSE relative to number of neurons in first and second hidden layer

	Number of neurons in first layer								
Number of neurons in second layer	—	5	10	15	20	25	30	35	40
	5	22	10.5	11.3	11.5	9	8.2	8.4	7.6
	10	14.3	10.8	9.5	10.2	7.9	7.8	7.8	7.8
	15	12.4	12.5	8.9	9.2	7.7	8.7	7.4	7.5
	20	17.2	10.4	8.5	7.8	7.5	7.5	7.2	9
	25	16.5	12.3	8.2	7.6	6.8	8.6	7.1	8.4
	30	16.2	12	9.2	7.1	7.2	7	8.3	7.8
	35	10.7	11	8.5	7.5	8.6	7.5	7	7.3
	40	11	9.1	7.7	9.3	7	6.9	7.3	7

and identifying the values obtained at strain rates below or above 0.1 s^{-1}. A strain rate of 0.1 s^{-1} was shown to be the threshold beyond which the strain rate effects become significantly more pronounced for UHPC materials.[79,80] The overall accuracy for predicting the cracking stresses and the tensile strength decreases for UHPC specimens tested under higher strain rates (over 0.1 s^{-1}), illustrated in Fig. 9. The prediction of the strain at the tensile strength, however,

Table 3—MLP-ANN model performance evaluation for predicting UHPC tensile properties

Data set	Tensile strength		Cracking stress		Strain at tensile strength	
	R^2	RMSE	R^2	RMSE	R^2	RMSE
Train	0.92	2.5	0.92	1.4	0.92	2.4
Test	0.91	2.4	0.81	1.8	0.92	2.7

does not appear to be impacted by the higher strain rates. As shown in Fig. 9 and reported in previous studies,[56-59,64] increased tensile strengths are obtained for higher strain rates. This is likely due to UHPC's dense structure and the increased bond strength between the cement matrix and the fiber reinforcement at elevated tensile strain rates.[80]

The model successfully differentiates between strain-hardening and strain-softening behavior based on the calculated values for the cracking stress and the tensile strength. Strain-softening mixtures result in equal values between the cracking stress and the tensile strength, whereas strain-hardening mixtures display a lower cracking stress compared to the tensile strength, as expected.

As shown in Fig. 9, the accuracy of the prediction algorithm was not significantly impacted by the assumptions made to characterize the database, including the use of the weighted average approach for UHPC mixtures containing fibers of the same type (straight, hooked, or twisted) but with different lengths and diameters. In addition, assumptions such as neglecting the number of bends in hooked fibers and threads in twisted fibers, not including the curing regime and duration, also had a minor effect on the accuracy of the predicted tensile properties.

The limitations of the proposed algorithm are largely related to the range of parameters covered in the database compiled. This model should not be expected to perform adequately for UHPC mixture designs that differ significantly from the ones analyzed herein. For example, there was insufficient data in the literature on the response of mixture designs that include basalt or cellulose fibers or metakaolin as SCMs. As such, the authors recommend against using the proposed model for these types of mixtures. However, should more data be available, the model could be expanded to include a broader range of mixture designs.

CONCLUSIONS

A multilayer perceptron artificial neural network (MLP-ANN) was developed for the prediction of cracking stress, tensile strength, and strain at tensile strength of various ultra-high-performance concrete (UHPC) mixtures. The following can be concluded:

1. The proposed MLP-ANN model proved to be an effective tool in predicting the tensile behavior of UHPC mixtures. An indication of the accuracy of the model consists of the coefficient of determination. The results of the predictions for the MLP-ANN algorithm showed R^2 values of 0.91, 0.81, and 0.92 for the tensile strength, cracking stress, and strain at tensile strength, respectively.

2. This procedure has the potential to decrease the effort, costs, and time to design a UHPC mixture without performing multiple mixture trials. This method should also be useful in the preliminary design and analysis of structural members by providing an initial estimate of the tensile strength based on the used UHPC mixture design.

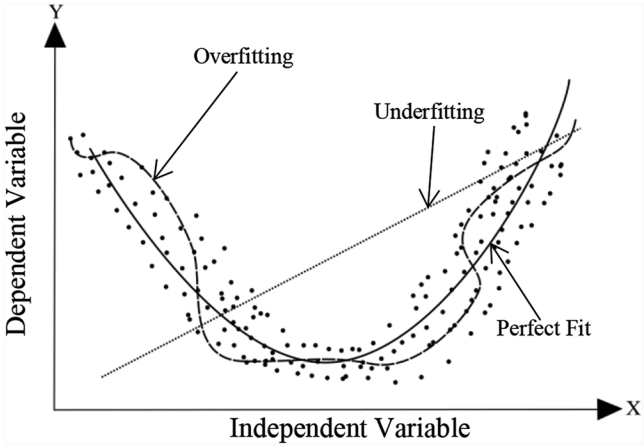

Fig. 8—Data fitting cases.

3. The model was developed to achieve the lowest mean squared error (MSE) in the development phase and the corresponding R^2 and root-mean-square error (RMSE) when comparing the experimental and predicted results. Employing a trial-and-error approach and testing various configurations of neurons ranging from 5 to 40 neurons, the optimum number of neurons converged to 25 neurons in each hidden layer, reaching the minimum MSE of 6.8.

4. The similarity of the R^2 and RMSE values between the training and test data sets indicates overfitting was not an issue in the prediction process, with no need for correction techniques such as regularization.

5. The correlation analysis and the test results displayed the strain rate's pronounced influence on the cracking stress and the tensile strength of UHPC mixtures. In contrast, the strain rate has minimal effect on the strain at tensile strength of the mixtures investigated in this study.

6. A nonlinear relationship was found between the fiber aspect ratio (fiber length/fiber diameter) and the UHPC tensile properties. As such, in this study, the fiber aspect ratio was disaggregated to capture the fact that the length and diameter of the fibers influence the tensile response differently and, therefore, were assigned different weights in the MLP-ANN model.

7. The mixture design constituents, including the water-cement ratio (w/c), high-range water-reducing admixture ratio, supplementary cementitious materials (SCMs) ratio, sand ratio, and fiber reinforcement characteristics, in addition to the tensile strain rate, proved to be sufficient in accurately predicting the tensile behavior of UHPC mixtures.

DATABASE AND ALGORITHM AVAILABILITY

The database, MLP-ANN algorithm, and user instructions are available for sharing upon request from the corresponding author.

AUTHOR BIOS

Amjad Y. Diab *is a PhD Student at The University of Texas at Austin, Austin, TX. His research interests include performance assessment and*

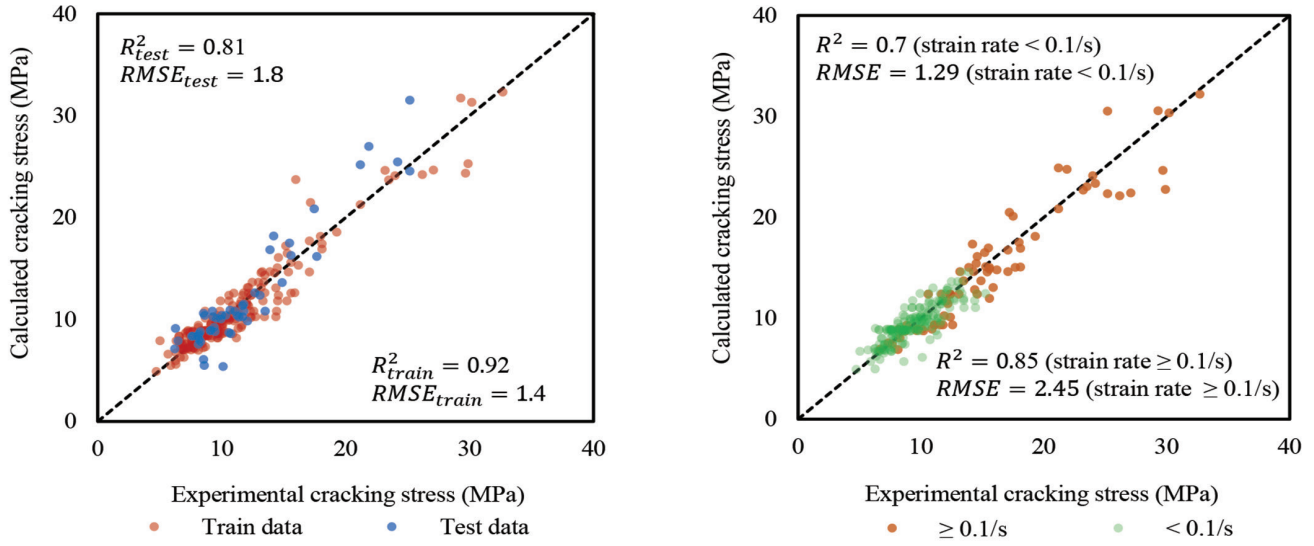

(a) Cracking stress

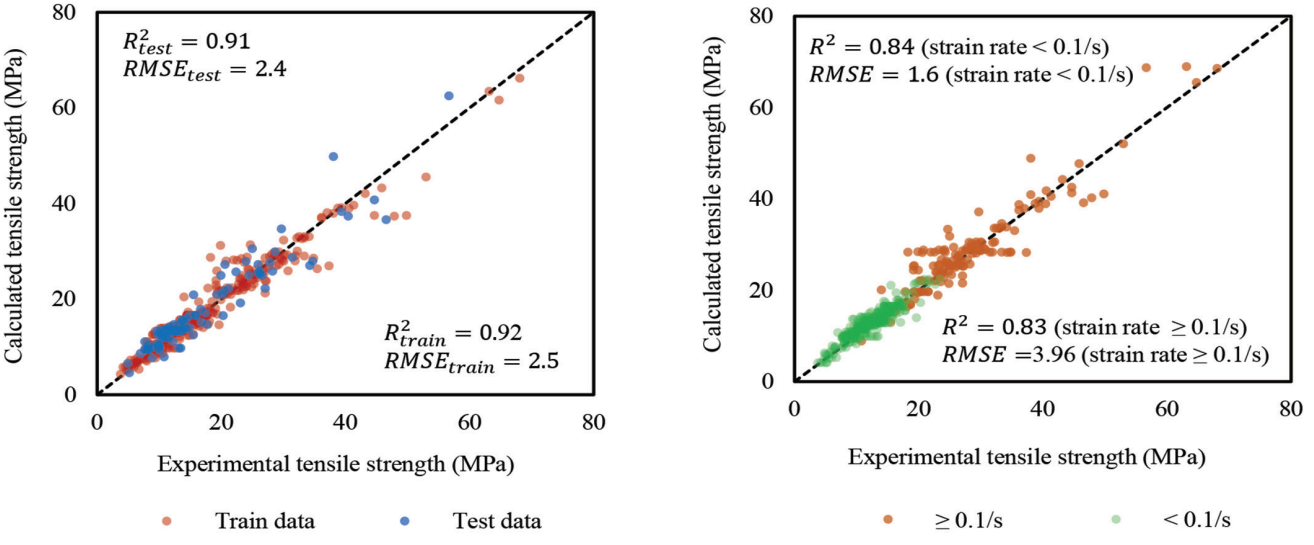

(b) Tensile strength

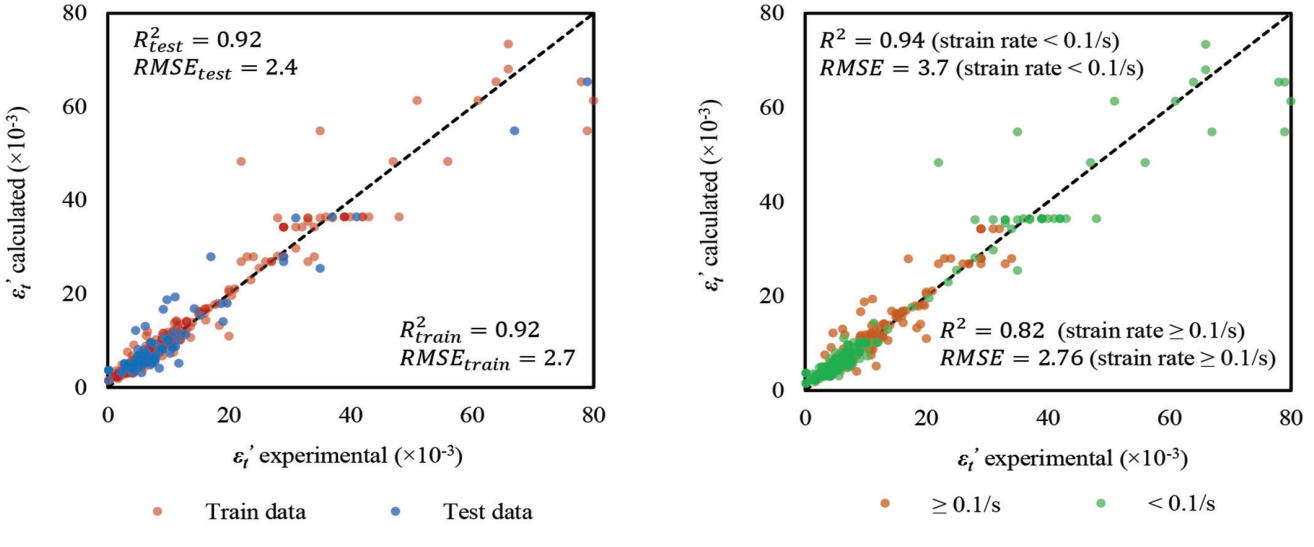

(c) Strain at tensile strength

Fig. 9—Comparison between experimental and calculated values of UHPC in terms of train-test and strain rates. (Note: 1.0 MPa = 145 psi.)

analysis of concrete structures, structural implications of deterioration mechanisms, and sustainability of concrete structures.

Anca C. Ferche *is an Assistant Professor in the Department of Civil, Architectural, and Environmental Engineering at The University of Texas at Austin. She received her PhD from the University of Toronto, Toronto, ON, Canada, in 2020. Her research interests include performance assessment and analysis of reinforced concrete structures, concrete deterioration mechanisms, and rehabilitation of structures.*

ACKNOWLEDGMENTS

The presented work was a part of a research project on UHPC sponsored by the Precast/Prestressed Concrete Institute (PCI). The authors would like to acknowledge the sponsorship from PCI for their funding and support for this project.

REFERENCES

1. AASHTO T 397-22, "Standard Method of Test for Uniaxial Tensile Response of Ultra-High Performance Concrete," American Association of State Highway and Transportation Officials, Washington, DC, 2022.

2. Toutlemonde, F.; Kretz, T.; Généreux, G.; Resplendino, J.; Pillard, W.; Guérinet, M.; and Rougeau, P., "French Standards for Ultra-High Performance Fiber-Reinforced Concrete (UHPFRC)," *High Tech Concrete: Where Technology and Engineering Meet*, D. A. Hordijk and M. Luković, eds., Springer, Cham, Switzerland, 2018, pp. 1601-1609.

3. Voo, Y. L.; Foster, S. J.; and Voo, C. C., "Ultra High-Performance Concrete Segmental Bridge Technology: Toward Sustainable Bridge Construction," *Journal of Bridge Engineering*, ASCE, V. 20, No. 8, 2015, pp. 1-12.

4. Azmee, N. M., and Shafiq, N., "Ultra-High Performance Concrete: From Fundamental to Applications," *Case Studies in Construction Materials*, V. 9, No. 197, 2018, pp. 1-15.

5. Haber, Z. B.; De la Varga, I.; Graybeal, B. A.; Nakashoji, B.; and El-Helou, R., "Properties and Behavior of UHPC-Class Materials," Report No. FHWA-HRT-18-036, Federal Highway Administration, Office of Infrastructure Research and Development, McLean, VA, 2018, 170 pp.

6. Richard, P., and Cheyrezy, M. H., "Reactive Powder Concretes With High Ductility and 200-800 MPa Compressive Strength," *Concrete Technology: Past, Present, and Future*, SP-144, P. K. Mehta, ed., American Concrete Institute, Farmington Hills, MI, 1994, pp. 507-518.

7. de Larrard, F., and Sedran, T., "Optimization of Ultra-High-Performance Concrete by the Use of a Packing Model," *Cement and Concrete Research*, V. 24, No. 6, 1994, pp. 997-1009.

8. Reiterman, P., "Influence of Metakaolin Additive and Nanoparticle Surface Treatment on the Durability of White Cement Based Concrete," *European Journal of Environmental and Civil Engineering*, V. 24, No. 13, 2020, pp. 2270-2283.

9. Cuenca, E.; Postolachi, V.; and Ferrara, L., "Cellulose Nanofibers to Improve the Mechanical and Durability Performance of Self-Healing Ultra-High-Performance Concretes Exposed to Aggressive Waters," *Construction and Building Materials*, V. 374, No. 4, Apr. 2023, Article No. 130785.

10. Kannikachalam, N. P.; di Summa, D.; Borg, R. P.; Cuenca, E.; Parpanesi, M.; De Belie, N.; and Ferrara, L., "Assessment of Sustainability and Self-Healing Performances of Recycled Ultra-High-Performance Concrete," *ACI Materials Journal*, V. 120, No. 1, Jan. 2023, pp. 117-132.

11. Cuenca, E.; Criado, M.; Giménez, M.; Alonso, M. C.; and Ferrara, L., "Effects of Alumina Nanofibers and Cellulose Nanocrystals on Durability and Self-Healing Capacity of Ultrahigh-Performance Fiber-Reinforced Concretes," *Journal of Materials in Civil Engineering*, ASCE, V. 34, No. 8, 2022, p. 04022154.

12. Cuenca, E.; Lo Monte, F.; Moro, M.; Schiona, A.; and Ferrara, L., "Effects of Autogenous and Stimulated Self-Healing on Durability and Mechanical Performance of UHPFRC: Validation of Tailored Test Method through Multi-Performance Healing-Induced Recovery Indices," *Sustainability*, V. 13, No. 20, 2021, p. 11386.

13. Cuenca, E., and Serna, P., "Autogenous Self-Healing Capacity of Early-Age Ultra-High-Performance Fiber-Reinforced Concrete," *Sustainability*, V. 13, No. 6, 2021, p. 3061.

14. Bonetti, R.; Bayrak, O.; Folliard, K.; and Drimalas, T., "A Framework for Determining Direct Tensile Properties of Ultra-High-Performance Concrete," *ACI Materials Journal*, V. 120, No. 2, Mar. 2023, pp. 87-95.

15. Park, S.; Wu, S.; Liu, Z.; and Pyo, S., "The Role of Supplementary Cementitious Materials (SCMs) in Ultra High Performance Concrete (UHPC): A Review," *Materials*, V. 14, No. 6, 2021, p. 1472.

16. Bharadwaj, K., "Supplementary Cementitious Materials in Portland-Limestone Cements," *ACI Materials Journal*, V. 119, No. 2, Mar. 2022, pp. 141-154.

17. Tadros, M.; Lawler, J.; El-Khier, M. A.; Gee, D.; and Kurt, A., "Implementation of Ultra-High Performance Concrete in Long-Span Precast Pretensioned Elements for Concrete Buildings and Bridges," *Precast/Prestressed Concrete Institute*, V. 10, No. 1, Jan. 2021.

18. Wille, K., and Naaman, A. E., "Fracture Energy of UHP-FRC Under Direct Tensile Loading," *Proceedings of the Seventh International Conference on Fracture Mechanics of Concrete and Concrete Structures (FraMCoS-7)*, B. H. Oh, ed., Jeju, South Korea, 2010, pp. 65-72.

19. Abrams, D. A., "Effect of Rate of Application of Load on the Compressive Strength of Concrete," *ASTM Proceedings*, V. 17, No. 1, 1917, pp. 364-377.

20. Bischoff, P. H., and Perry, S. H., "Compressive Behaviour of Concrete at High Strain Rates," *Materials and Structures*, V. 24, No. 6, 1991, pp. 425-450.

21. Suaris, W., and Shah, S. P., "Strain-Rate Effects in Fibre-Reinforced Concrete Subjected to Impact and Impulsive Loading," *Composites*, V. 13, No. 2, 1982, pp. 153-159.

22. Gopalaratnam, V. S., and Shah, S. P., "Properties of Steel Fiber Reinforced Concrete Subjected to Impact Loading," *ACI Journal Proceedings*, V. 83, No. 1, Jan.-Feb. 1986, pp. 117-126.

23. Wang, Z.-L.; Liu, Y.-S.; and Shen, R. F., "Stress-Strain Relationship of Steel Fiber-Reinforced Concrete Under Dynamic Compression," *Construction and Building Materials*, V. 22, No. 5, 2008, pp. 811-819.

24. Bindiganavile, V., and Banthia, N., "Impact Response of the Fiber-Matrix Bond in Concrete," *Canadian Journal of Civil Engineering*, V. 32, No. 5, 2005, pp. 924-933.

25. Pyo, S.; Wille, K.; and El-Tawil, S., "Strain Rate Dependent Properties of Ultra High Performance Fiber Reinforced Concrete (UHP-FRC) Under Tension," *Cement and Concrete Composites*, V. 56, 2015, pp. 15-24.

26. Wille, K.; Xu, M.; and El-Tawil, S., "Dynamic Impact Factors of Strain Hardening UHP-FRC Under Direct Tensile Loading at Low Strain Rates," *Materials and Structures*, V. 49, No. 4, 2016, pp. 1351-1365.

27. Park, S. H.; Kim, D. J.; and Kim, S. W., "Investigating the Impact Resistance of Ultra-High-Performance Fiber-Reinforced Concrete Using an Improved Strain Energy Impact Test Machine," *Construction and Building Materials*, V. 125, No. 1, 2016, pp. 145-159.

28. Malvar, L. J., and Ross, C. A., "Review of Strain Rate Effects for Concrete in Tension," *ACI Materials Journal*, V. 95, No. 6, Nov.-Dec. 1998, pp. 735-739.

29. Cadoni, E.; Meda, A.; and Plizzari, G. A., "Tensile Behaviour of FRC under High Strain-Rate," *Materials and Structures*, V. 42, No. 9, 2009, pp. 1283-1294.

30. Rossi, P., "A Physical Phenomenon Which Can Explain the Mechanical Behaviour of Concrete under High Strain Rates," *Materials and Structures*, V. 24, No. 6, 1991, pp. 422-424.

31. Rossi, P.; van Mier, J. G. M.; and Boulay, C., "The Dynamic Behaviour of Concrete: Influence of Free Water," *Materials and Structures*, V. 25, No. 9, 1992, pp. 509-514.

32. ASTM C496/C496M-17, "Standard Test Method for Splitting Tensile Strength of Cylindrical Concrete Specimens," ASTM International, West Conshohocken, PA, 2017, 5 pp.

33. ASTM C1609/C1609M-19a, "Test Method for Flexural Performance of Fiber-Reinforced Concrete (Using Beam With Third-Point Loading)," ASTM International, West Conshohocken, PA, 2019, 9 pp.

34. Kim, J. J., and Taha, R., "M. "Experimental and Numerical Evaluation of Direct Tension Test for Cylindrical Concrete Specimens," *Advances in Civil Engineering*, V. 2014, No. 1, 2014, pp. 1-8.

35. Maalej, M., and Li, V. C., "Flexural/Tensile-Strength Ratio in Engineered Cementitious Composites," *Journal of Materials in Civil Engineering*, ASCE, V. 6, No. 4, 1994, pp. 513-528.

36. Naaman, A. E., and Reinhardt, H. W., "Proposed Classification of HPFRC Composites Based on Their Tensile Response," *Materials and Structures*, ASCE, V. 39, No. 5, 2007, pp. 547-555.

37. Abellán-García, J., "Four-Layer Perceptron Approach for Strength Prediction of UHPC," *Construction and Building Materials*, V. 256, No. 1, 2020, p. 119465.

38. Abellán-García, J., "Artificial Neural Network Model for Strength Prediction of Ultra-High-Performance Concrete," *ACI Materials Journal*, V. 118, No. 4, July 2021, pp. 3-14.

39. Ghafari, E.; Bandarabadi, M.; Costa, H.; and Júlio, E., "Design of UHPC Using Artificial Neural Networks," *Brittle Matrix Composites*, A. M. Brandt, J. Olek, M. A. Glinicki, and C. K. Y. Leung, eds., Woodhead Publishing, Sawston, UK, 2012, pp. 61-69.

40. Abellán García, J.; Fernandez Gomez, J.; and Torres Castellanos, N., "Properties Prediction of Environmentally Friendly Ultra-High-Performance Concrete Using Artificial Neural Networks," *European Journal of Environmental and Civil Engineering*, V. 26, No. 6, 2022, pp. 2319-2343.

41. Mostafa, S. A.; Ahmed, N.; Almeshal, I.; Tayeh, B. A.; and Elgamal, M. S., "Experimental Study and Theoretical Prediction of Mechanical

Properties of Ultra-High-Performance Concrete Incorporated With Nanorice Husk Ash Burning at Different Temperature Treatments," *Environmental Science and Pollution Research International*, V. 29, 2022, pp. 75380-75401.

42. Mahjoubi, S.; Meng, W.; and Bao, Y., "Auto-Tune Learning Framework for Prediction of Flowability, Mechanical Properties, and Porosity of Ultra-High-Performance Concrete (UHPC)," *Applied Soft Computing*, V. 115, 2022, p. 108182.

43. Zakaria, M.; Shebany, M.; and Sarhan, S., "Artificial Neural Network: A Brief Overview," *International Journal of Engineering Research and Applications*, V. 4, No. 2, 2014, pp. 7-12.

44. Gunasekara, C.; Atzarakis, P.; Lokuge, W.; Law, D. W; and Setunge, S., "Novel Analytical Method for Mix Design and Performance Prediction of High Calcium Fly Ash Geopolymer Concrete," *Polymers*, V. 13, No. 6, 2021, pp. 1-21.

45. Rosenblatt, F., "The Perceptron: A Probabilistic Model for Information Storage and Organization in the Brain," *Psychological Review*, V. 65, No. 6, 1958, pp. 386-408.

46. Estebon, M. D., "Perceptrons: An Associative Learning Network," Virgina Tech, Blacksburg, VA, 1997.

47. Asteris, P. G.; Skentou, A. D.; and Bardhan, A., "Predicting Concrete Compressive Strength Using Hybrid Ensembling of Surrogate Machine Learning Models," *Cement and Concrete Research*, V. 145, No. 1, 2021, pp. 1-23.

48. Ramchoun, H.; Amine, M.; and Idrissi, J., "Multilayer Perceptron: Architecture Optimization and Training," *International Journal of Interactive Multimedia and Artificial Intelligence*, V. 4, No. 1, 2016, pp. 1-26.

49. Bircanoğlu, C., and Arıca, N. "A Comparison of Activation Functions in Artificial Neural Networks," 2018 26th Signal Processing and Communications Applications Conference (SIU), İzmir, Turkey, 2018, pp. 1-4.

50. Rumelhart, D. E.; Hinton, G. E.; and Williams, R. J., "Learning Representations by Back-Propagating Errors," *Nature*, V. 323, No. 6088, 1986, pp. 533-536.

51. Hoang, N.-D.; Nguyen, Q.-L.; and Tran, X.-L., "Automatic Detection of Concrete Spalling Using Piecewise Linear Stochastic Gradient Descent Logistic Regression and Image Texture Analysis," *Complexity*, V. 2019, No. 1, 2019, pp. 1-14.

52. Awolusi, T. F.; Oke, O. L.; and Akinkurolere, O. O., "Performance Comparison of Neural Network Training Algorithms in the Modeling Properties of Steel Fiber Reinforced Concrete," *Heliyon*, V. 5, No. 1, 2019, pp. 1-27.

53. Su, C., and Wang, W., "Concrete Cracks Detection Using Convolutional Neural Network Based on Transfer Learning," *Mathematical Problems in Engineering*, V. 2020, No. 1, 2020, pp. 1-10.

54. Collier, M., and Urdiales, H. "Scalable Deep Unsupervised Clustering with Concrete GMVAEs," arXiv, 2019, pp. 1-5.

55. Moriasi, D. N.; Arnold, J. G.; Van Liew, M. W.; Bingner, R. L.; Hamel, R. D.; and Veith, T. L., "Model Evaluation Guidelines for Systematic Quantification of Accuracy in Watershed Simulations," *Transactions of the ASABE*, V. 50, No. 3, 2007, pp. 885-900.

56. Gupta, P.; Seetharaman, A.; and Raj, J. R., "The Usage and Adoption of Cloud Computing by Small and Medium Businesses," *International Journal of Information Management*, V. 33, No. 5, 2013, pp. 861-874.

57. Park, J. K.; Kim, S.-W.; and Kim, D. J., "Matrix-Strength-Dependent Strain-Rate Sensitivity of Strain-Hardening Fiber-Reinforced Cementitious Composites under Tensile Impact," *Composite Structures*, V. 162, No. 1, 2017, pp. 313-324.

58. Ranade, R.; Li, V. C.; and Heard, W. F., "Tensile Rate Effects in High Strength-High Ductility Concrete," *Cement and Concrete Research*, V. 68, No. 1, 2015, pp. 94-104.

59. Tran, N. T., and Kim, D. J., "Synergistic Response of Blending Fibers in Ultra-High-Performance Concrete under High Rate Tensile Loads," *Cement and Concrete Composites*, V. 78, No. 1, 2017, pp. 132-145.

60. Tran, N. T.; Tran, T. K.; and Kim, D. J., "High Rate Response of Ultra-High-Performance Fiber-Reinforced Concretes under Direct Tension," *Cement and Concrete Research*, V. 69, No. 1, 2015, pp. 72-87.

61. Chun, B., and Yoo, D.-Y., "Hybrid Effect of Macro and Micro Steel Fibers on the Pullout and Tensile Behaviors of Ultra-High-Performance Concrete," *Composites Part B: Engineering*, V. 162, No. 1, 2019, pp. 344-360.

62. Bian, C., and Wang, J.-Y., "Mechanical and Damage Mechanisms of Reinforced Ultra-High-Performance Concrete Under Tensile Loading," *Construction and Building Materials*, V. 226, 2019, pp. 259-279.

63. Wang, J.-Y., and Guo, J.-Y., "Damage Investigation of Ultra High-Performance Concrete under Direct Tensile Test Using Acoustic Emission Techniques," *Cement and Concrete Composites*, V. 88, No. 1, 2018, pp. 17-28.

64. Yoo, D.-Y., and Kim, M.-J., "High Energy Absorbent Ultra-High-Performance Concrete with Hybrid Steel and Polyethylene Fibers," *Construction and Building Materials*, V. 209, No. 1, 2019, pp. 354-363.

65. Pyo, S.; El-Tawil, S.; and Naaman, A. E., "Direct Tensile Behavior of Ultra-High Performance Fiber Reinforced Concrete (UHP-FRC) at High Strain Rates," *Cement and Concrete Research*, V. 88, No. 1, 2016, pp. 144-156.

66. Le Hoang, A., and Fehling, E., "Influence of Steel Fiber Content and Aspect Ratio on the Uniaxial Tensile and Compressive Behavior of Ultra-High-Performance Concrete," *Construction and Building Materials*, V. 153, No. 1, 2017, pp. 790-806.

67. Kamal, A.; Kunieda, M.; and Ueda, N., "Evaluation of Crack Opening Performance of a Repair Material with Strain Hardening Behavior," *Cement and Concrete Composites*, V. 30, No. 10, 2008, pp. 863-871.

68. Ranade, R.; Li, V. C.; Stults, M. D.; Heard, W. F.; and Rushing, T. S., "Composite Properties of High-Strength, High-Ductility Concrete," *ACI Materials Journal*, V. 110, No. 4, July-Aug. 2013, pp. 413-422.

69. Yu, K.-Q.; Lu, Z.-D.; and Dai, J.-G., "Direct Tensile Properties and Stress-Strain Model of UHP-ECC," *Journal of Materials in Civil Engineering*, ASCE, V. 32, No. 1, 2020, pp. 1-13.

70. Park, S. H.; Kim, D. J.; and Ryu, G. S., "Tensile Behavior of Ultra High Performance Hybrid Fiber Reinforced Concrete," *Cement and Concrete Composites*, V. 34, No. 2, 2012, pp. 172-184.

71. Yavaş, A.; Hasgul, U.; and Turker, K., "Effective Fiber Type Investigation on the Shear Behavior of Ultrahigh-Performance Fiber-Reinforced Concrete Beams," *Advances in Structural Engineering*, V. 22, No. 7, 2019, pp. 1591-1605.

72. Voss, M. S.; Riding, K. A.; and Alrashidi, R. S., "Comparison between Direct Tension, Four-Point Flexure, and Simplified Double-Punch Tests for UHPC Tensile Behavior," *Journal of Materials in Civil Engineering*, ASCE,V. 34, No. 9, 2022, pp. 1-12.

73. Delen, D.; Sharda, R.; and Bessonov, M., "Identifying Significant Predictors of Injury Severity in Traffic Accidents Using a Series of Artificial Neural Networks," *Accident Analysis & Prevention*, V. 38, No. 3, 2006, pp. 434-444.

74. Rajagopalan, G., *A Python Data Analyst's Toolkit: Learn Python and Python-Based Libraries with Applications in Data Analysis and Statistics*, Apress, Berkeley, CA, 2014.

75. Nayak, S. K., and Ojha, A. C., "Data Leakage Detection and Prevention: Review and Research Directions," *Machine Learning and Information Processing: Proceedings of ICMLIP*, 2019.

76. Shabtai, A.; Elovici, Y.; and Rokach, L., *A Survey of Data Leakage Detection and Prevention Solutions*, Springer Science & Business Media, New York, 2012.

77. Bilbao, I., and Bilbao, J., "Overfitting Problem and the Over-Training in the Era of Data: Particularly for Artificial Neural Networks," 2017 Eighth International Conference on Intelligent Computing and Information Systems (ICICIS), Cairo, Egypt, V. 1, 2017, pp. 173-177.

78. Ying, X., "An Overview of Overfitting and its Solutions," *Journal of Physics: Conference Series*, V. 1168, No. 2, 2019, pp. 1-6.

79. Hentz, S.; Donzé, F. V.; and Daudeville, L., "Discrete Element Modelling of Concrete Submitted to Dynamic Loading at High Strain Rates," *Computers & Structures*, V. 82, No. 29-30, 2004, pp. 2509-2524.

80. Thomas, R. J., and Sorensen, A. D., "Review of Strain Rate Effects for UHPC in Tension," *Construction and Building Materials*, V. 153, 2017, pp. 846-856.

Table A1—Database description

Ref.	Specimens	*w/c*	FA/C	Sa/C	SF/C	GGBFS/C	S/B	SF	SFL	SFD	HF	HFL	HFD	TF	TFL	TFD	PE	SR	DTS	CTS	SC
Unit	N/A	%	%	%	%	%	%	%	mm	mm	%	mm	mm	%	mm	mm	%	S-1 ($\times 10^{-3}$)	MPa	MPa	με
Park et al.[57]	53	20 to 35	0 to 25	100 to 125	0 to 25	0	0.9 to 6.7	1	13	0.2	1	30	0.375	0	0	0	0	0.3 to 161,000	10.4 to 43.2	N/A	4 to 2.1
Pyo et al.[25]	36	22	0	134	25	0	0.5	0 to 3	0 to 25	0 to 0.4	0	0	0	0 to 3	18 to 25	0.3	0	0.1 to 100	8.11 to 24.1	6.22 to 14.6	1.7 to 48
Reanade et al.[58]	36	20.8	0	70	39	0	1.8	0	0	0	0	0	0	0	0	0	2.14	0.1 to 10,000	14.5 to 22.8	6.6 to 14.6	22 to 48
Tran and Kim[59]	46	20	0	110	25	0	6.7	0 to 1.5	0 to 30	0 to 0.3	0 to 1.5	30	0.375	0 to 1.5	24.3 to 30	0.27 to 0.3	0	0.167 to 37,000	9.2 to 39.4	N/A	2.3 to 20
Tran et al.[60]	72	20	0	110	25	0	6.7	0 to 1.5	0 to 19	0 to 0.2	0	0	0	0 to 1.5	20	0.2	0	0.167 to 23,700	10.1 to 37.4	N/A	44,606
Wille et al.[26]	36	19	0	92	25	0	6.7	0 to 3	0 to 13	0 to 0.2	0 to 3	30	0.38	0 to 3	18	0.3	0	0.1 to 100	11.1 to 24.9	7.3 to 17.1	44,659
Chun and Yoo[61]	12	25	0	110	25	0	2	0 to 2	13 to 30	0.2 to 0.3	0 to 2	30	0.38	0 to 2	30	0.3	0	0.083	12.25 to 17.68	5.91 to 11.35	44,720
Bian and Wang[62]	6	20	0	164	30	0	1.3	1 to 2	16	0.2	0	0	0	0	0	0	0	0.2	9.3 to 10.6	10.1 to 12	0.2 to 4.5
Wang and Guo[63]	9	20	0	134	30	0	0.5	1.5 to 2.5	13	0.2	0	0	0	0	0	0	0	0.2	7.7 to 10.8	7.7 to 13	0.2 to 4
Yoo and Kim[64]	12	20	0	110	25	0	6.5	0 to 2	0 to 19.5	0 to 0.2	0	0	0	0 to 2	30	0.3	0 to 1.5	0.3	12 to 20.3	4.76 to 9.98	44,671
Pyo et al.[65]	38	22	0	134	25	0	0.5	0 to 3	0 to 25	0 to 0.4	0	0	0	0 to 3	25	0.3	0	66,000 to 146,000	19.9 to 68.1	13.2 to 32.7	44,640
Le Hoang and Fehling[66]	36	20	0	147	21	0	3	1.5 to 3	9 to 20	0.15 to 0.25	0	0	0	0	0	0	0	0.067	7.71 to 14.4	5.05 to 15.3	N/A
Wille and Naaman[18]	7	22	0	129	25	0	0.54	0 to 2.5	0 to 13	0 to 0.2	0 to 2	30	0.38	0 to 2	0 to 30	0 to 0.3	0	0.33	8 to 15.5	N/A	1.7 to 6.1
Kamal et al.[67]	3	20	0	12.5	25	0	2	0.5 to 1.5	6	0.012	0	0	0	0	0	0	0	2	3.8 to 10	N/A	28 to 58
Ranade et al.[68]	6	21	0	60 to 97	39	0	0.009 to 0.024	0	0	0	0 to 3.6	0 to 30	0 to 0.55	0	0	0	0 to 2	0.03	10.4 to 14.5	N/A	1.8 to 35
Yu et al.[69]	14	33	0	71	21.4	107	0.005	0	0	0	0	0	0	0	0	0	1.5 to 3	0.2	10.29 to 17.89	8.15 to 12.09	22 to 80
Park et al.[70]	16	20	0	110	25	0	0.067	0 to 2	13 to 24	0.2 to 0.3	0 to 1	0 to 62	0 to 0.775	0 to 1	0 to 30	0 to 0.3	0	0.04	8.08 to 18.56	7.09 to 11.35	0.9 to 6.4
Yavaş et al.[71]	16	29	0	157	20	40	0.016	0 to 1.5	0 to 13	0 to 0.16	0 to 1.5	0 to 60	0 to 0.9	0	0	0	0	0.07	4.2 to 9.4	N/A	N/A
Voss et al.[72]	10	21	0	97.5	9.7	19.3	0.03	0 to 2.78	0 to 13	0 to 0.2	0	0	0	0 to 2.78	0 to 13	0 to 0.5	0	0.3	4.9 to 7.0	N/A	N/A

Note: Abbreviations are provided in Table 1.

NEW Symposium Publications from ACI

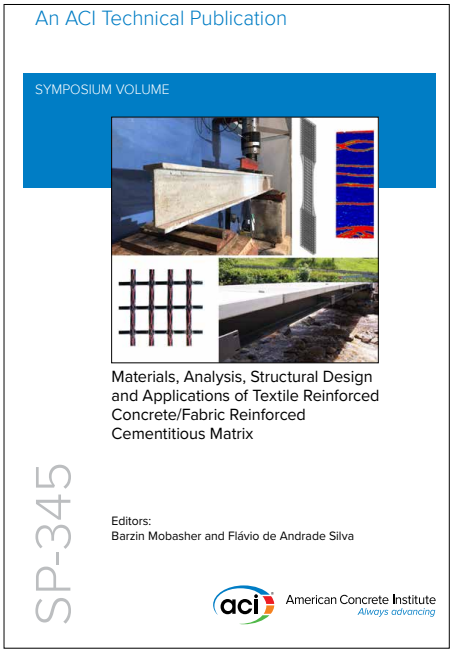

SP-345: Materials, Analysis, Structural Design and Applications of Textile Reinforced Concrete/Fabric Reinforced Cementitious Matrix

Several state-of-the-art sessions on textile-reinforced concrete/fabric-reinforced cementitious matrix (TRC/FRCM) were organized by ACI Committee 549 in collaboration with RILEM TC MCC during the ACI Fall 2019 Convention in Cincinnati, OH, and the ACI Virtual Technical Presentations in June 2020. The forum provided a unique opportunity to collect information and present knowledge in the field of TRC and FRCM as sustainable construction materials.

Available in PDF format: $69.50
(FREE to ACI members)

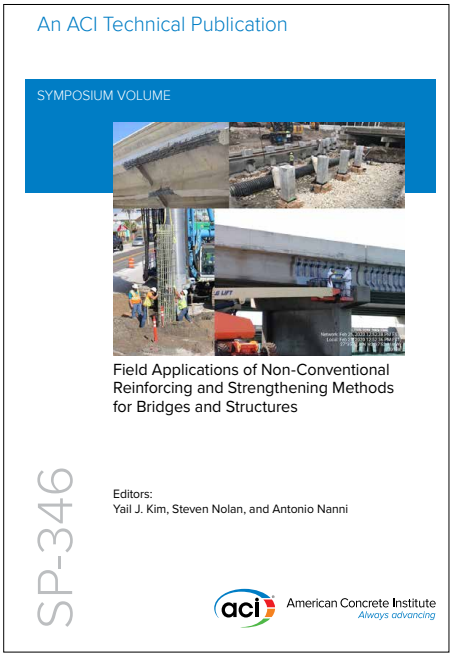

SP-346: Field Applications of Non-Conventional Reinforcing and Strengthening Methods for Bridges and Structures

A sustainable built environment requires a comprehensive process from material selection through to reliable management. Although traditional materials and methods still dominate the design and construction of our civil infrastructure, nonconventional reinforcing and strengthening methods for concrete bridges and structures can address the functional and economic challenges facing modern society.

Available in PDF format: $69.50
(FREE to ACI members)

American Concrete Institute
+1.248.848.3700 • www.concrete.org